Supermolecular organization of photosystem II and its associated light-harvesting antenna in Arabidopsis thaliana

Yakushevska, AE; Jensen, PE; Keegstra, W; van Roon, H; Scheller, HV; Boekema, EJ; Dekker, JP; Yakushevska, Alevtyna E.; Jensen, Poul E.; Scheller, Henrik V.

Published in:
European Journal of Biochemistry

DOI:
10.1046/j.0014-2956.2001.02505.x

Publication date:
2001

Eur. J. Biochem. **268,** 6020–6028 (2001) © FEBS 2001

Supermolecular organization of photosystem II and its associated light-harvesting antenna in *Arabidopsis thaliana*

Alevtyna E. Yakushevska[1], Poul E. Jensen[2], Wilko Keegstra[1], Henny van Roon[3], Henrik V. Scheller[2], Egbert J. Boekema[1] and Jan P. Dekker[3]

[1]*Department of Biophysical Chemistry, Groningen Biomolecular Sciences and Biotechnology Institute, University of Groningen, Nijenborgh, Groningen, the Netherlands;* [2]*Plant Biochemistry Laboratory, Department of Plant Biology, The Royal Veterinary and Agricultural University, Copenhagen, Denmark;* [3]*Faculty of Sciences, Division of Physics and Astronomy, Vrije Universiteit, Amsterdam, the Netherlands*

The organization of *Arabidopsis thaliana* photosystem II (PSII) and its associated light-harvesting antenna (LHCII) was studied in isolated PSII–LHCII supercomplexes and native membrane-bound crystals by transmission electron microscopy and image analysis. Over 4000 single-particle projections of PSII–LHCII supercomplexes were analyzed. In comparison to spinach supercomplexes [Boekema, E.J., van Roon, H., van Breemen, J.F.L. & Dekker, J.P. (1999) *Eur. J. Biochem.* **266**, 444–452] some striking differences were revealed: a much larger number of supercomplexes from *Arabidopsis* contain copies of M-type LHCII trimers. M-type trimers can also bind in the absence of the more common S-type trimers. No binding of L-type trimers could be detected. Analysis of native membrane-bound PSII crystals revealed a novel type of crystal with a unit cell of 25.6 × 21.4 nm (angle 77°), which is larger than any of the PSII lattices observed before. The data show that the unit cell is built up from $C_2S_2M_2$ supercomplexes, rather than from C_2S_2M supercomplexes observed in native membrane crystals from spinach [Boekema, E.J., Van Breemen, J.F.L., Van Roon, H. & Dekker, J.P. (2000) *J. Mol. Biol.* **301**, 1123–1133]. It is concluded from both the single particle analysis and the crystal analysis that the M-type trimers bind more strongly to PSII core complexes in *Arabidopsis* than in spinach.

Keywords: photosystem II; *Arabidopsis thaliana*; electron microscopy; supercomplex; light-harvesting.

Photosystem II (PSII) is a pigment-protein complex embedded in the thylakoid membrane of higher plants, algae and cyanobacteria. It catalyses a sunlight-driven process, splitting water into protons and molecular oxygen. This multisubunit protein complex consists of more than 25 structurally and functionally distinct subunits organized hierarchically [1,2]. First is the PSII core complex, of which the chlorophyll-containing CP43 and CP47 proteins and the reaction center are the most important components. The latter consists of D1 and D2 proteins, which generate the redox potential required to drive the water splitting reaction. The structure of the core complex has been solved at 3.8 Å resolution by the X-ray diffraction of three-dimensional crystals of PSII from *Synechococcus elongatus* [3]. The core complex, which normally exists as a dimer, contains extrinsic proteins attached to the lumenal surface. These proteins, which arise from the oxygen-evolving complex (OEC), have an apparent molecular mass of 33 (Mn-stabilizing protein), 23 and 17 kDa, respectively, and are necessary for maintaining the water oxidation process.

The recently reported structure of PSII from *Synechococcus elongatus* revealed, in detail, the spatial organization of the protein subunits and pigment molecules within PSII [3]. The arrangement of all the large subunits and most of the small subunits has been assigned, as well as the position of cytochrome b_{559} and cytochrome c_{550} and the localization of the manganese cluster that catalyzes oxidation of water. This knowledge will also aid understanding of the structure of the green plant core PSII, which has a very similar structure. Several small PSII core subunits such as PsbL, PsbK, and PsbW have been proposed to be involved in the dimerization of the PSII [4,5]. The first two have been tentatively assigned, but other small components required for stabilizing dimeric PSII, such as phosphatidyl glycerol [6], cannot be solved at the present resolution.

Second is the peripheral antenna, which is involved in the absorption of light and subsequent energy transfer to the reaction center. In higher plants and algae it consists of various pigment-containing proteins encoded by the 'cab' gene family [7]. The major light-harvesting complex II (LHCII) complex is trimeric, consists of the Lhcb1-3 proteins and contains chlorophyll a/b and carotenoids. Its structure was solved by electron crystallography at 3.4 Å resolution [8]. The minor complexes, Lhcb4 (CP29), Lhcb5 (CP26), Lhcb6 (CP24) are monomeric and also contain chlorophyll a/b and carotenoids. They are involved in mediating excitation energy transfer from the LHCII trimers to the PSII core complex.

Correspondence to E. J. Boekema, Department of Biophysical Chemistry, Groningen Biomolecular Sciences and Biotechnology Institute, University of Groningen, Nijenborgh 4, 9747 AG Groningen, the Netherlands. Fax: + 31 50 363 4800, Tel.: + 31 50 363 4225, E-mail: boekema.chem.rug.nl

Abbreviations: PSII, photosystem II; PSI, photosystem I; LHCII, light-harvesting antenna; OEC, oxygen evolving complex; S, strongly bound; M, moderately bound; L, loosely bound; α-DM, *n*-dodecyl-α-D-maltoside.

(Received 25 May 2001, revised 30 July 2001, accepted 10 September 2001)

The components mentioned above together comprise the PSII–LHCII supercomplexes [1,9]. Biochemical evidence suggests that on average, about eight trimers of LHCII are present per PSII core dimer [10], but only a part of the LHCII complexes are directly bound to the PSII core complexes. Various LHCII trimers have been distinguished by the strength of binding to the core complex. The following classification was proposed based on the strength of binding of LHCII to the core part of the supercomplex: S, strongly bound LHCII; M, moderately bound LHCII and L, loosely bound LHCII [11,12]. The number of constituents is indicated after the corresponding letter; thus C_2 represents a dimeric core complex and C_2S_2 represents a dimeric core with two strongly bound LHCII trimers.

The structural organization of the core PSII complexes and multiple types of associations of the core complex with light-harvesting antennae (supercomplexes) have been investigated by electron microscopy (EM) [9,11–13] and cross-linking studies [14]. A three-dimensional structure of a supercomplex from spinach, calculated at 24 Å resolution by EM and single particle analysis of ice-embedded preparations [13], revealed the position and the tetrameric structure of the OEC, as well as the location of the extrinsic OEC proteins on the lumenal surface of the membrane. Cross-linking studies suggested the specific location of the three minor antenna complexes Lhcb-4, Lhcb-5 and Lhcb-6 [14].

It is not known in detail how these supercomplexes, nonbound LHCII trimers, and possibly the cytochrome b_6/f complex are arranged in the grana membrane or how these proteins from adjacent grana membranes interact to get membrane stacks. The LHCII trimers serve as the main stabilizers in the formation of appressed grana membranes. However, *chlorina* mutants from barley, despite the greatly reduced levels of these proteins, still have grana. It was consequently concluded that PSII core proteins can also induce membrane oppression [15]. Numerous freeze-etch and freeze-fracture EM studies indicate that PSII complexes have a tendency to form ordered domains within the grana membrane, although noncrystalline domains usually seem to dominate in wild-type plants [16]. However, these techniques do not precisely reveal the type of PSII complex, because of the lack of resolution [1]. Crystallinity can be studied in greater detail in isolated, paired inside-out grana membranes purified by gel-filtration chromatography. Investigation of negatively stained paired membrane fragments from spinach by EM and image analysis revealed the motif of two different types of lattices [17]. The most dominant one consisted of C_2S_2M supercomplexes, the other contained C_2S_2 supercomplexes. Crystalline domains of two adjacent layers also show some specificity in their association, as preferential angles between two lattices are frequently observed.

In this report, we present details on the structural organization of PSII from wild type *Arabidopsis thaliana* by EM and image analysis. Two approaches were followed: the periodic approach (analysis of crystalline membrane fragments) indicated a new type of crystal lattice composed of $C_2S_2M_2$ PSII–LHCII supercomplexes; and the a-periodic approach (analysis of 4000 projections of single PSII particles) indicated the presence of large numbers of PSII–LHCII supercomplexes with attached M-type LHCII trimers.

MATERIALS AND METHODS

Isolation of inside-out grana and single particles

PSII–LHCII supercomplexes and native grana membranes were isolated from thylakoid membranes from *A. thaliana*, essentially as described previously for spinach thylakoid membranes [18], and prepared immediately for EM. For the PSII–LHCII supercomplexes, thylakoid membranes at a chlorophyll concentration of 1.4 mg·mL^{-1} were partially solubilized with *n*-dodecyl-α-D-maltoside (α-DM) at a final concentration of 0.6% at 4 °C in a buffer containing 20 mM Bistris (pH 6,5) and 5 mM $MgCl_2$. After centrifuging for 3 min at 9000 r.p.m. in an Eppendorf table-top centrifuge the supernatant was filtered through a 0.45-μm filter in order to remove large fragments. The solubilized fractions were purified by gel-filtration chromatography, using a superdex 200 HR 10/30 column as described previously [18]. The fractions eluting at 20 min were used for single particles analysis. For the native grana membranes, the thylakoid membranes were solubilized as above, but with only 0.3% α-DM. The first fraction with green material, eluting at 17 min, was used for EM analysis.

Electron microscopy and image analysis

Samples of purified single particles and membranes were negatively stained using the droplet method with 2% uranyl acetate and imaged using a Philips CM10 electron microscope at 52 000 × magnification. Negatively stained specimens were prepared on glow discharged carbon-coated copper grids as described previously [11]. Electron micrographs were digitized with a Kodak Eikonix Model 1412 CCD camera with a step size of 25 μm, corresponding to a pixel size of 0.485 nm at the specimen level. Particles were extracted from negatives and analyzed with IMAGIC software [19] and GRONINGEN IMAGE PROCESSING ('GRIP') software (W. Keegstra, unpublished results). A total of 20 000 single particle images from 105 negatives were obtained by selecting all discernable particles. The analysis of these images started with multireference alignment [20,21], followed by multivariate statistical analysis [20] and classification [21]. The data set was then split into 90 classes, rejecting 15% of the particles. Only classes containing PSII particles were selected for further analysis. Classes containing similar particles were pooled together. This procedure resulted in eight classes containing 4249 PSII particles of various types. The quality of these eight data sets was ascertained by subsequent alignment and classification. The best 40–50% of particles from each data set were finally summed. The resolution of the images was measured as described previously [22].

From 29 digitized negatives with paired inside-out membranes with crystalline arrays, we selected 656 partially overlapping fragments with a size of 144 × 144 pixels (or 700 × 700 nm). The crystal fragments were analyzed following an a-periodic procedure, as for single particles, in a similar way as for spinach crystals [17]. To examine the positions of individual PSII complexes in adjacent layers, the layers were separated and individually filtered with standard Fourier-peak filtering. The resolution of final sums was evaluated from the IQ values of structure factors

obtained by two-dimensional Fourier transformation, as previously described [23].

RESULTS

Analysis of single, isolated PSII–LHCII supercomplexes

In order to investigate the supermolecular organization of PSII from *A. thaliana* the thylakoid membranes were solubilized with α-DM under stacking conditions, basically as described before for spinach thylakoids by Van Roon *et al.* [18]. In spinach, this approach resulted in a selective solubilization of all components from the stromal and margin membranes, leaving the grana virtually intact as paired membranes with an average diameter of about 360 nm [17,18]. In *Arabidopsis*, however, a solubilization procedure with even a two times smaller amount of detergent resulted in almost complete disruption of the membranes, as indicated by a strongly decreased content of large aggregates eluting at 17 min in the gel filtration chromatography and a strongly increased content of particles eluting at 20 min, where PSII–LHCII complexes are expected [24], together with photosystem I monomers (PSI-200) and aggregates of PSI [18]. This interpretation was confirmed by EM and image analysis.

To investigate the structure and numbers of various types of supercomplexes, a data set of 20 000 single particle projections was selected from the fractions eluting at 20 min. After repeated cycles of multireference alignment, multivariate statistical analysis and classification of the 20 000 projections, 15% were automatically rejected during the last classification step. From the remaining 85%, ≈ 54% of the projections could be assigned, either to PSI monomers and aggregates (33%; not shown) or to PSII (21%; see below). Some of the nonassigned projections were assumed to represent wrong aligned particles. A total of 4249 projections assigned to PSII represent dimeric PSII core complexes ('C_2') to which variable numbers of two different types of LHCII trimers (the 'S' type and 'M' type) are associated, forming so-called PSII–LHCII supercomplexes [9,11,12]. Seven main types of PSII–LHCII supercomplexes were found (Fig. 1); their relative abundance is listed in Table 1. The resolution of the images was ≈ 2.6 nm.

Four out of these seven types of supercomplexes have previously been found in spinach [11,12,25]. They consist of $C_2S_2M_2$, C_2S_2M, C_2SM and C_2S_2 configurations and are depicted in Fig. 1A–D, respectively. An interesting result in the present data set was the presence of three new types of PSII–LHCII particles (Fig. 1E–G). They together comprised ≈ 10% of the PSII data set. Image analysis revealed that they basically consist of a C_2 core part (as in Fig. 1H) and S-type and M-type trimers (as in Fig. 1A), but that some of these M-trimers could be attached without the presence of neighboring S-trimers. For instance, the supercomplex of Fig. 1F lacks a S-trimer in the left upper part of the complex. We named it MC_2S, to discriminate from the C_2SM supercomplex (Fig. 1C). The projection of Fig. 1E is similar but has an additional M-trimer attached to the lower left tip. A rather small number of supercomplexes has no S-trimers attached at all (Fig. 1G). These three types of supercomplex particles were not previously observed in spinach. To exclude the possibility that they had been previously overlooked, we re-examined the data sets of complexes obtained from solubilized spinach PSII membranes by using those novel types of particles (Fig. 1E–G) each as a reference. There were no particles matching these references, indicating their total absence from spinach. On the other hand, there is no detectable amount of L-type LHCII trimers attached to the *Arabidopsis* supercomplexes, in contrast to spinach, where low numbers were found [12]. Moreover, no particles from the type I and type II megacomplexes were found. Finally, we only detected three particles of the type III megacomplex [12]. The absence of megacomplexes could in part be caused by the fractions that were analyzed; they are probably more abundant in earlier fractions.

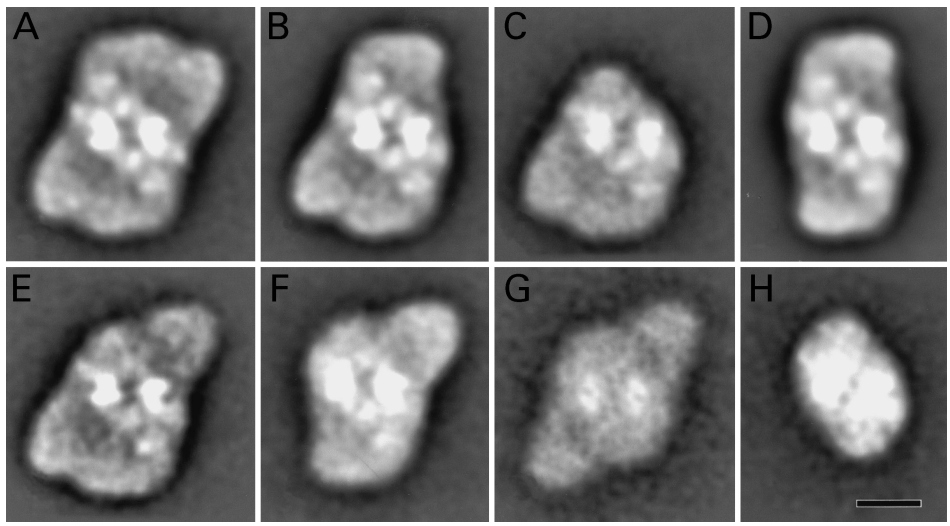

Fig. 1. Results of multireference alignment and classification of top-view projections of PSII complexes from *Arabidopsis* wild type. (A) Average of the best 218 $C_2S_2M_2$ projections. (B) Average of 290 C_2S_2M projections. (C) Average of 175 C_2SM projections. (D) Average of 300 C_2S_2 projections. (E) Average of 164 C_2SM_2 projections. (F) Average of 190 MC_2S projections. (G) Average of 34 C_2M_2 projections. (H) Average of 100 C_2 core complexes. Twofold rotational symmetry was imposed on the images of A, D and G. The scale bar is 10 nm.

Table 1. Relative occurrence of PSII–LHCII supercomplexes and megacomplexes in solubilized PSII membranes from *A. thaliana* and spinach. Taken from [12].

Complex	No. assigned projections	% Projections	
		Arabidopsis	Spinach
Total	4249	100	100
C_2S_2	1134	26.7	70.6
C_2SM	828	19.5	7.2
C_2S_2M	1142	26.9	14.6
$C_2S_2M_2$	747	17.6	0.9
C_2M_2	37	0.9	0
C_2SM_2	164	38	0
MC_2S	194	4.5	0
Mega I ($C_4S_4M_{2-4}$)	0	0	2.8
Mega II ($C_4S_4M_{2-4}$)	0	0	1.3
Mega III (C_4S_4)	3	0.1	0.3
Total S	7232	85.2	100
Total M	3665	43.2	16.5
Total L	0	0	0.7

Conformational differences between supercomplex projections

A more detailed investigation of the particle projections from *Arabidopsis* shows some unexpected changes in the association of the M-type trimers, if neighboring S-type trimers were absent. Absence of such a trimer can lead to a significant rearrangement in the binding position the M-type trimer, as demonstrated in Fig. 2B–D, which shows the contoured versions of the new types of projections. The rearrangements are visualized by comparing the density maximums of the $C_2S_2M_2$ particle (Fig. 2A) with the positions of these densities in the new types of supercomplexes. At the site of the tentative CP24 subunit, the positions of these density maximums differ substantially from the observed positions on the C_2SM_2, MC_2S and C_2M_2 supercomplexes (indicated by yellow dots in Fig. 2B–D). The shifts are also obvious if the place of the cleft between the S-type and M-type trimers, as indicated by the red arrow in Fig. 2A, is superposed on the supercomplexes of Fig. 2B–D. In the C_2M_2 particle (Fig. 2D) there is an inward shift of CP24 of ≈ 2.7 nm and the M-trimer is also simultaneously shifted in an upward direction (see red arrow in Fig. 2D). In the case of the C_2SM_2 particle, the density attributed to the CP24 subunits moved ≈ 3.4 nm inward and an even stronger shift of the M-trimer was visible. However, the shifts in the MC_2S particle are less pronounced (Fig. 2C). These differences might indicate one or more

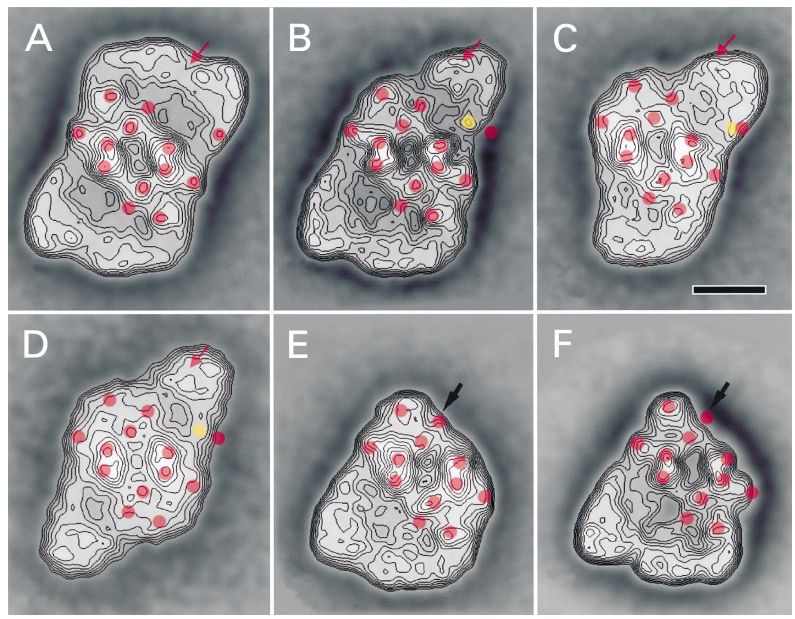

Fig. 2. Comparison of positions of M-type trimers in various types of *Arabidopis* and spinach PSII–LHCII supercomplexes. (A) Contoured version of the image of Fig. 1A. (B–D) Contoured versions of the images of Fig. 1E,G. (E) contoured image of Fig. 1C. (F) Contoured image from 200 spinach C_2SM supercomplexes (generated from data sets in [12]). The position of some density maxima in the $C_2S_2M_2$ projection of (A) have been indicated by red dots. These positions have been overlaid on the other images, if present. This has also been performed for the position of the red arrow, which indicates in (A) the position of the interface between the upper S-type and M-type trimers. The yellow dots in (B) to (D) indicate the place where the density, marked in (A) by the upper right red dot, is actually observed and thus point to larger or smaller changes in the position of the upper M-trimer upon absence of an adjacent S-type trimer. The black arrow in (E) and (F) indicates the site where the C_2SM supercomplexes from *Arabidopsis* and spinach have their largest difference. The scale bar is 10 nm.

successive stages of an increasing displacement. On the other hand, no differences between the upper tips of the images of Fig. 2B,C can be expected if the subunit composition is the same. Unfortunately, the causes for the discrepancies in shifts cannot be solved by further classification, given the limited numbers of these projections.

In addition to these differences in the peripheral antennae, there are smaller differences between the core parts of *Arabidopsis* and spinach. Because the resolution in the C_2 core complexes is limited, these differences are only well observed in the C_2SM type of PSII particle (Fig. 2E,F). The red dots in Fig. 2E,F near the black arrows mark the place with the largest difference.

Analysis of two-dimensional crystals

The study of negatively stained intact inside-out paired membranes can give interesting insight into the packing and ordering of PSII supercomplexes, because the row-like arranged PSII core parts can be easily averaged due to their strongly protruding extrinsic subunits. In comparison to spinach grana membranes, however, the grana membranes of *Arabidopsis* appeared to be more easily disrupted by α-DM. At a detergent concentration of 0.3%, which is four times less than used to prepare spinach paired membranes, most observed membranes were seen to be severely damaged. On the other hand, almost all of the remaining intact membranes showed strong periodicity in the arrangement of PSII complexes (Fig. 3A,B). The crystallinity was present in both superimposed layers (Fig. 3A,B). For calculating a two-dimensional projection map, information of 29 recorded crystals was combined. The standard approach for crystals, which is the Fourier analysis, was not used (see below). Instead, a noncrystallographic approach was used, as it better handles small crystals with severe lattice imperfections [17]. The crystals were divided in 656 overlapping small fragments for analysis by repeated alignments, multivariate statistical analysis and classification, in a very similar way as carried out previously with spinach inside-out paired membranes [17]. To extract as much information as possible from both layers, the fragments were additionally processed in their mirrored version. In this way, information from the upper layer could also be extracted, although this layer was usually less well negatively stained and preserved than the lower layer that sticks to the carbon support film. This addition was not performed in the analysis of the spinach crystals, where crystallinity in one specific part of a layer did not strongly correlate to crystallinity in the other one [17]. After a final classification step (not shown) of the 1312 fragments, a final group of 450 fragments from the best classes was obtained (Fig. 4A). In this group, ≈ 68% of the fragments originated from the lower layer and 32% from the mirrored upper layer. The final group of 450 crystal fragments shows a handedness that is opposite to the handedness of the single particles, where the extrinsic subunits are positioned away from the carbon support film, but otherwise shows very similar structural features, especially in the core part region. The unit cell or repeating motif of the crystal was

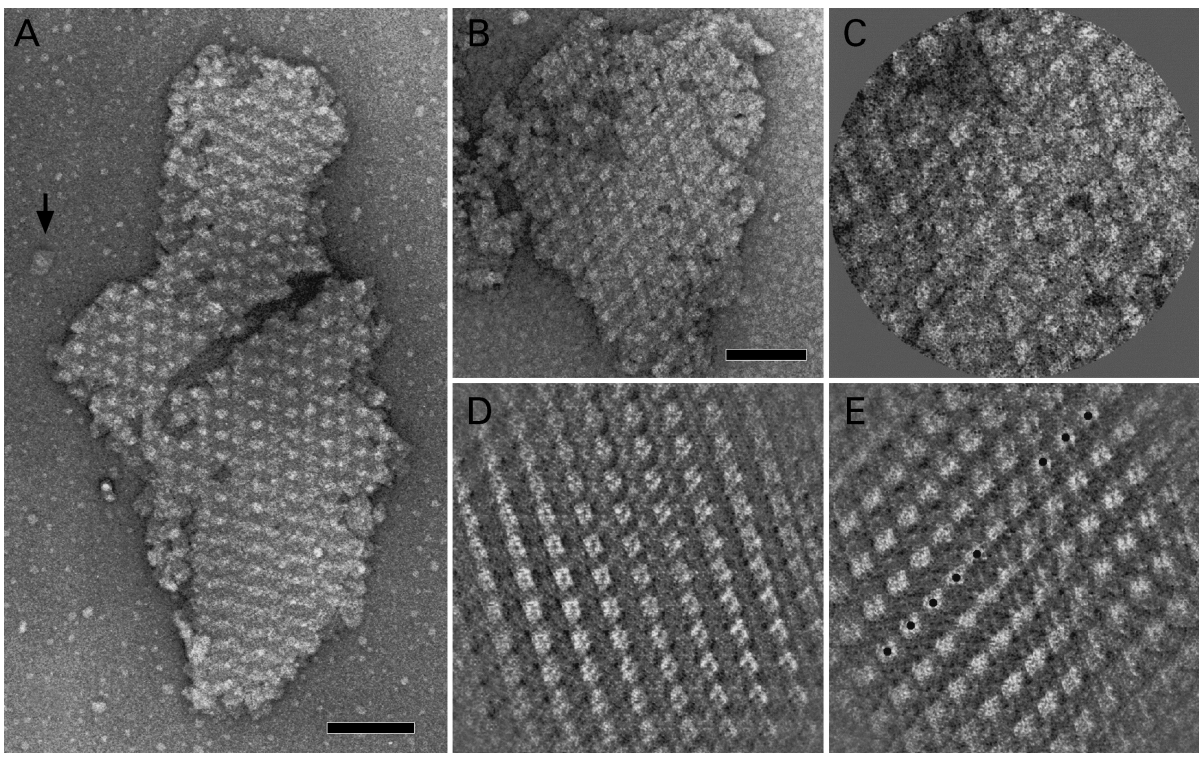

Fig. 3. Electron micrographs and filtering of a selected crystalline area of PSII supercomplexes in paired inside-out grana membranes. (A,B) Membranes negatively stained with 2% uranyl acetate. (C) Selected area of image (B), used for Fourier-peak-filtering of the two superimposed layers. (D,E) Images of separated layers after filtering. The black dots in (E) mark the centers of individual core complexes and indicate a dislocation in the crystal packing of one particular layer. The arrow in (A) points to a single $C_2S_2M_2$ supercomplex. The space bars represent 100 nm.

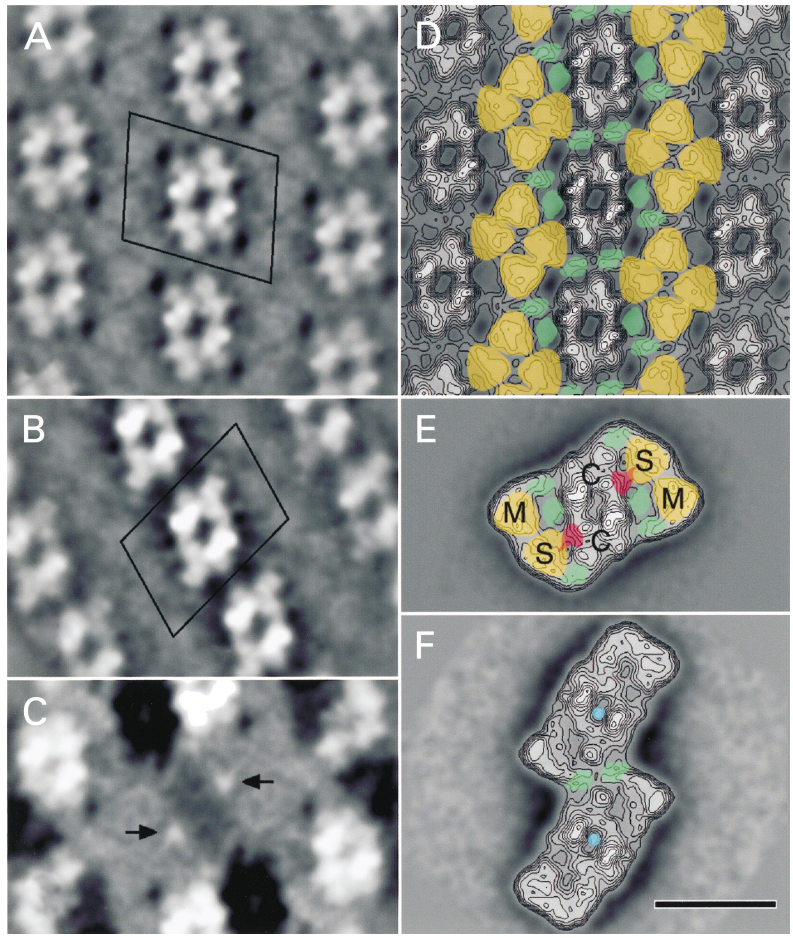

Fig. 4. Final result of image analysis of two-dimensional crystalline and comparison. (A) Sum of 450 aligned crystal fragments from *Arabidopsis*; the unit cell has been indicated; (B) sum of 900 aligned crystal fragments from spinach (from [17]) with the central PSII dimer in the same position as in (A), the unit cell has been indicated; (C) Difference image between (A) and (B), arrows point to the site of strongest difference. (D) Image form (A) with contours; positions of S-type and M-type LHCII trimers indicated in yellow and positions of CP29, CP26 and CP24 indicated in green. (E) Image of the $C_2S_2M_2$ supercomplex (from Fig. 1A) in equivalent position, with the dimeric part ('c'), the S-type and M-type LHCII trimers ('s'and 'm') indicated in yellow, the CP29, CP26 and CP24 areas in green and the strongest difference area from image (C) indicated in red; (F) image of type III megacomplex (from [11]) in similar rotational position as in (A). The blue dots mark the centers of two adjacent PSII complexes as in (A) and the green areas indicate two CP26 positions as in (A). The images of (A) to (D) have been mirrored after image analysis, to facilitate comparison with the single particle averages. The space bar represents 20 nm.

25.6 × 21.4 nm with an angle of 77° between the crystal axes (Fig. 4A). Fourier-transformation indicated that structural details were present up to 2.5 nm in resolution [23].

Relative positions of supercomplexes in inside-out paired membranes

If analysis of crystalline arrays of paired membranes was focussed on the superposition of both layers, it became clear that the interaction of the rows of PSII complexes of adjacent layers was to some extend specific. Of 58 crystals examined, the majority showed that the angle between rows of PSII complexes from the superposed layers fell into a small range; it was either ≈ 32°± 2° (mean ± SD, $n = 16$) or ≈ 58°± 3° ($n = 33$). Crystalline arrays showing different angles had an overall smaller degree of ordering. Examples of crystals with overlapping rows of PSIl complexes differing in rotation by 32° and 58° are presented in Fig. 3A and B, respectively. However, image analysis of these and several other crystals showed that the restricted rotational freedom in attachment does not imply that the super-complexes become associated to each other in a similar way all over the crystal. The largest crystals, such as the one shown in Fig. 3A, show this very clearly. It can be seen that the Moiré pattern, which is the resulting motif from the overlap of two crystals making an angle, gradually changes. The upper and lower part of the crystal show about the same type of Moiré pattern (and thus of the type of overlap), which differs substantially from the central part. In the center of this crystal, the PSII core parts of both layers are more strongly overlapping in projection. A similar pattern with overlapping core complexes in the center of the paired membranes was observed in other crystals of the 32°-type. Another aspect of the lateral freedom in the interaction of the two layers is demonstrated by the crystal of Fig. 3B. This was shown by Fourier filtering, a technique that can separate two superposed layers differing in rotational position by selecting only those peaks in the Fourier-transformed image that belong to one specific layer. The processed selected central part of this crystal (Fig. 3C) shows this very well. After Fourier filtering, which reduces noise and separates the layers, a crystal defect could be detected in one of the layers resulting in a translational shift with a magnitude of about half a unit cell (Fig. 3E). Similar types of imperfections within one layer were observed in other analyzed inside-out paired of membranes of the 58°-type.

DISCUSSION

In this report, we present an analysis of membrane-bound crystalline PSII and isolated PSII–LHCII supercomplexes from *Arabidopsis*. One of the ultimate aims of such an analysis is the detection of subunits crucial to regulation mechanisms, such as PsbS [26], by comparing the sets of

isolated supercomplexes or complete (crystalline) membranes from wild-type and mutants lacking such subunits. Furthermore, a close comparison to the spinach data [1,9,11–13,25] is useful for detecting specific structural features of *Arabidopsis* PSII. With the appearance of the first complete genomic sequence of a plant, *Arabidopsis* [27], new perspectives for further investigation of all individual photosynthetic proteins, becomes available.

Analysis of the *Arabidopsis* crystals shows the presence of only one crystal form (Fig. 4A), which has unit cell dimensions of 25.6 × 21.4 nm (angle 77°). It covers a surface area of 534 nm^2. The crystal is larger than any of the PSII lattices observed previously. The projection map clearly reveals the positions of two LHCII trimers flanking each side of a dimeric PSII core complex (Fig. 4A). Because the position of these trimers strongly resembles the positions of S- and M-type LHCII trimers as found in the single $C_2S_2M_2$ supercomplex projection (Fig. 4E), we fitted these trimers, together with the remaining peripheral antenna components CP29, CP26 and CP24, into the crystal lattice (Fig. 4D). From this fitting it can be concluded that the crystal arrays consist of $C_2S_2M_2$ particles. Further evidence comes from the observation that only $C_2S_2M_2$ single particles can be frequently found around the crystals (Fig. 3A). In contrast, the previously analyzed large-sized crystals from spinach [17] had a differently shaped unit cell of 27.3 × 18.3 nm (Fig. 4B), which is also 11% smaller in surface. We previously noticed that the spinach crystals were too small to contain a $C_2S_2M_2$ particle and it was concluded that they were composed of C_2S_2 M particles [17]. The present analysis of *Arabidopsis* crystals, where M-type trimers are directly observed, confirms this assignment.

The *Arabidopsis* crystals show a marked preference in the way the two layers are attached. The rows of core complexes in the two layers make an angle of either ≈ 32° or 58°. A rotational preference was also observed in the spinach crystals: preferential angles of 3° or 46° were found [17]. As the PSII complexes from which the two different types of crystals are built up only differ in the peripheral antennae, we speculate that the LHCII trimers, rather than the core complexes, determine the way of interaction between the two layers, which leads to the preference in rotational position. If the LHCII trimers strive to optimize association and overlap, this would automatically lead to strong overlap of core complexes in at least a part (the center) of the paired membranes. This is essentially also the case in the previously studied spinach crystals, but in that case large domains of LHCII trimers without attached core complexes form an additional type of variation [17]. Although the LHCII trimers appear to be important to induce preferential stacking of crystalline membranes, other factors might be relevant as well, such as the lipid composition of the membranes and the protein/lipid ratio.

The analysis of isolated *Arabidopsis* PSII–LHCII supercomplexes showed the presence of relatively high amounts of M-type LHCII trimers. This is evident from a comparison of the relative numbers of those types of supercomplexes, which were also present in the previously analyzed 12755 spinach supercomplexes (Table 1 [12]); the number of $C_2S_2M_2$ projections is significantly (20 times) larger. Furthermore, we noticed that the numbers of C_2S_2 and C_2S_2M particles are about equal, whereas in spinach the larger part was formed by the C_2S_2 particles. The analysis of isolated *Arabidopsis* PSII–LHCII supercomplexes also

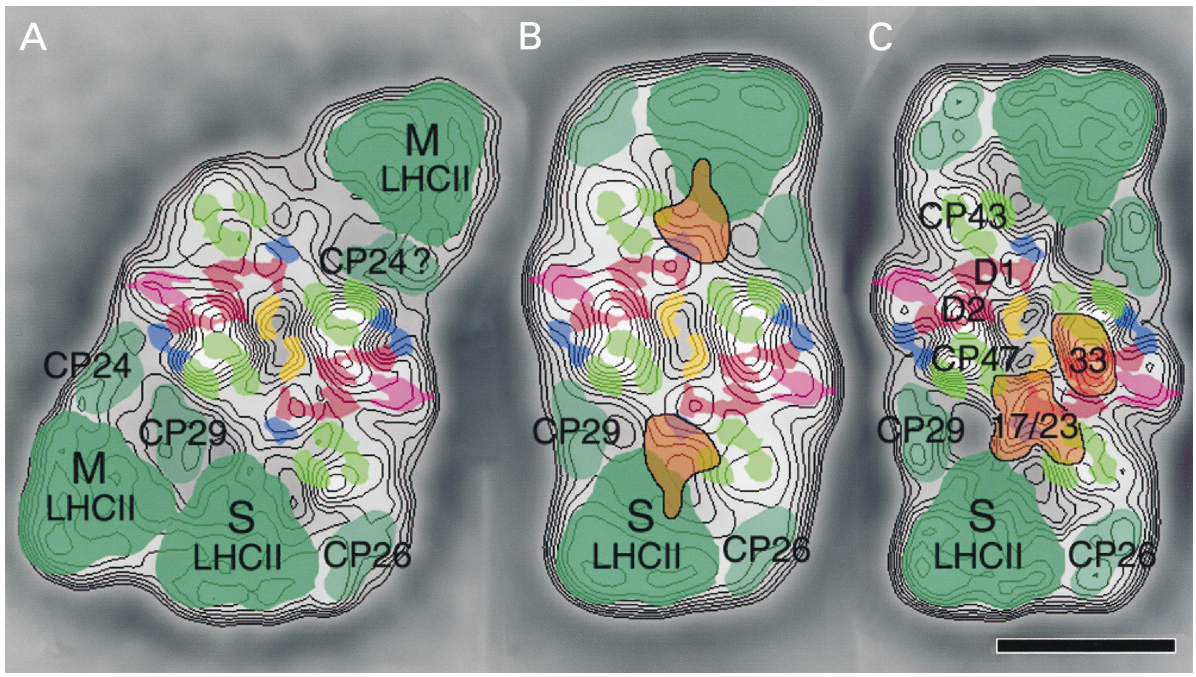

Fig. 5. Modeling of subunit densities in supercomplex projection maps. (A,B) The C_2SM_2 and C_2S_2 supercomplexes of *Arabidopsis*. (C) The C_2S_2 supercomplex from spinach (from [12] with core subunit densities from [5]). The position of the upper M-type LHCII trimer in (A) indicates a major shift for the attached minor LHC subunit (possibly a CP24 subunit), but otherwise the core parts and the lower half of the peripheral antennas in (A–C) are rather similar. The difference areas from Fig. 4E are reproduced in (B) and overlap of these densities suggests that these areas, assigned to the extrinsic subunits occupy a larger space than the extrinsic 33 and 17/23 kDa subunit areas as shown in (C) (from [12]). The space bar is 10 nm.

showed for the first time the presence of M-type trimers in the absence of adjacent S-type trimers (Fig. 2). Such particles were completely absent in the spinach data sets. The best resolved particle was the C_2SM_2 supercomplex. Fitting of subunits densities into this projection (Fig. 5A) revealed that the upper M-type trimer occupies the correct amount of expected space, but that the adjacent minor LHC subunit, possibly CP24, must have rearranged its position dramatically because otherwise no space is left over. Apparently, the absence of the adjacent S-type trimer strongly influences the binding of the more peripheral M-type trimers. This situation is reminiscent to our experiments with the specific removal of the extrinsic subunits, which had a profound influence on the position of the S-type trimer and CP29 [25]. There is, however, no evidence that the *Arabidopsis* single particles have a reduced number of S-type trimers because of the loss or absence of extrinsic subunits. On the contrary, a close comparison of the features from the central supercomplex particles in the averaged native crystals from *Arabidopsis* and spinach indicates additional masses for *Arabidopsis* at the two sites where the S-type trimers are attached to the core complex (Figs 4C and 5B). The fact that these masses seem to overlap with the S-type trimers suggests that they should be considered as extrinsic subunits. These masses, which were previously assigned as the 17 and 23 kDa extrinsic subunits [28]), are easily lost in spinach but are apparently stronger when attached to *Arabidopsis* supercomplexes. This is also reflected in the comparison of density profiles of isolated C_2SM supercomplexes (Fig. 2E,F). The averaged *Arabidopsis* C_2S_2M supercomplex shows more density at about the same site as the spinach supercomplex, as became clear from the crystal difference map (Fig. 4C). If indeed the *Arabidopsis* PSII complexes have stronger bound extrinsic subunits, as suggested from the crystal difference map (Fig. 4C), then it is unlikely that they are responsible for the overall lower stability of bound S-type trimers in *Arabidopsis*.

Another difference between the isolated *Arabidopsis* and spinach supercomplexes has to do with the further association into megacomplexes. No particles of the type I and II megacomplexes were observed in *Arabidopsis*, and only a few type III complexes were present (Table 1), although we did not examine the fractions where such particles tend to accumulate. The observation of only type III megacomplexes could be of coincidence, but we would like to point out that in the latter type of megacomplex, the packing of the supercomplex is very similar to the packing in the crystals, as is shown in the fitting of crystal features into the spinach type III megacomplex (Fig. 4F). Finally, the CP26 area in all *Arabidopsis* supercomplexes was somewhat the same. No variation at the CP26 position was detected (Fig. 1A–F). On the other hand, a substantial number of the spinach projections lacked this tip completely, although this absence did not influence the supercomplex structure [12,25].

The analysis of *Arabidopsis* PSII–LHCII supercomplexes has contributed further to the evidence for the structural complexity of the association of the peripheral antenna of PSII. Some of this variation could originate from slight differences in the solubilization and purification process. Nevertheless we can conclude that both the single particle analysis and the crystal analysis indicate the presence of larger numbers of associated M-type LHCII trimers. A strong argument for the *in vivo* presence of larger amounts of the M-type LHCII trimers is the fact that in contrast to spinach, where C_2S_2M as well as C_2S_2-containing crystals were found, *Arabidopsis* seems to exclusively contain $C_2S_2M_2$ crystals. The finding that native *Arabidopsis* plants contain a higher degree of M-type LHCII trimers, and thus an overall larger antenna associated to PSII–LHCII supercomplexes, is of interest for further studies focussed on subunits important for state transitions and nonphotochemical quenching, such as PsbS [26]. As there is evidence that PsbS is not present in the C_2S_2 supercomplexes [29], larger supercomplexes, as found in *Arabidopsis*, might be more suited for structural localization of PsbS.

ACKNOWLEDGEMENTS

Support from the Dutch Scientific foundation NWO/ALW to E. J. B and J. P. D and from the Danish National Research Foundation to P. E. J. and H. V. S. is gratefully acknowledged.

REFERENCES

1. Hankamer, B., Barber, J. & Boekema, E.J. (1997) Structure and membrane organization ofphotosystem II in green plants. *Annu. Rev. Plant Physiol. Plant Mol. Biol.* **48**, 641–671.
2. Hankamer, B., Morris, E.P. & Barber, J. (1998) Revealing the structure of the oxygen-evolving core dimer ofphotosystem II by cryoelectron crystallography. *Nat. Struct. Biol.* **6**, 560–564.
3. Zouni, A., Witt, H.-T., Kern, J., Fromme, P., Krauss, N., Saenger, W. & Orth, P. (2001) Crystal structure ofphotosystem II from *Synechoccus elongatus* at 3.8 Å resolution. *Nature* **409**, 739–743.
4. Zheleva, D., Sharma, J., Panico, M., Morris, H.R. & Barber, J. (1998) Isolation and characterization of monomeric and dimeric CP47-reaction center photosystem II complexes. *J. Biol. Chem.* **273**, 16122–16127.
5. Shi, L.-X., Lorkovic, Z.J., Oelmüller, R. & Schröder, W.P. (2000) The low molecular mass PsbW protein is involved in the stabilization of the dimeric photosystem II complex in *Arabidopsis thaliana*. *J. Biol. Chem.* **275**, 37945–37950.
6. Kruse, O., Hankamer, B., Konczak, C., Gerle, C., Morris, E., Radunz, A., Schmid, G.H. & Barber, J. (2000) Phosphatidylglycerol is involved in the dimerisation of photosystem II. *J. Biol. Chem.* **275**, 6509–6514.
7. Jansson, S. (1994) The light-harvesting chlorophyll a/b-binding proteins. *Biochim. Biophys. Acta* **1184**, 1–19.
8. Kühlbrandt, W., Wang, D.N. & Fujiyoshi, Y. (1994) Atomic model of plant light-harvesting complex by electron microscopy. *Nature* **367**, 614–621.
9. Boekema, E.J., Hankamer, B., Bald, D., Kruip, J., Boonstra, A.F., Barber, J. & Rögner, M. (1995) Supramolecular structure of the photosystem II complex from green plants and cyanobacteria. *Proc. Natl Acad. Sci. USA* **92**, 175–179.
10. Peter, G.F. & Thornber, J.P. (1991) Biochemical composition and organization of higher plant photosystem II light-harvesting pigment-proteins. *J. Biol. Chem.* **266**, 16745–16754.
11. Boekema, E.J., Van Roon, H., Calkoen, F., Bassi, R. & Dekker, J.P. (1999) Multiple types of association of photosystem II and its light-harvesting antenna in partially solubilized photosystem II membranes. *Biochemistry* **38**, 2233–2239.
12. Boekema, E.J., Van Roon, H., Van Breemen, J.F.L. & Dekker, J.P. (1999) Supramolecular organization of photosystem II and its light-harvesting antenna in partially solubilized photosystem II membranes. *Eur. J. Biochem.* **266**, 444–452.
13. Nield, J., Orlova, E.V., Morris, E.P., Gowen, B., Van Heel, M. &

Barber, J. (2000) 3D map of the plant photosystem II supercomplex obtained by cryoelectron microscopy and single particle analysis. *Nat. Struct. Biol.* **7**, 44–47.
14. Harrer, R., Bassi, R., Testi, M.G. & Schäfer, C. (1998) Nearest-neighbour analysis of a photosystem II complex from *Marchantia polymorpha* L. (liverworth) which contains reaction centre and antenna proteins. *Eur. J. Biochem.* **255**, 196–205.
15. Simpson, D.J. (1979) Freeze-fracture studies on barley plastid membranes III. Location of the light-harvesting chlorophyll protein. *Carlsberg Res. Commun.* **44**, 305–336.
16. Staehelin, L.A., Armond, P.A. & Miller, K.R. (1977) Chloroplast membrane organization at the supermolecular level and its functional implication. *Brookhaven Symposia Biol.* **28**, 278–315.
17. Boekema, E.J. & Van Breemen, J.F.L., Van Roon, H. & Dekker J.P. (2000) Arrangement of photosystem II in crystalline macrodomains within the thylakoid membrane of green plant chloroplasts. *J. Mol. Biol.* **301**, 1123–1133.
18. Van Roon, H. Van Breemen, J.F.L., De Weerd, F.L., Dekker J.P. & Boekema, E.J. (2000) Solubilization of green plant thylakoid membranes with *n*-dodecyl-α,D-maltoside. Implications for the structural organization of the photosystem II, photosystem I ATP synthase and cytochrome b_6/f complexes. *Photosynth. Res.* **64**, 155–166.
19. Harauz, G., Boekema, E. & Van Heel, M. (1988) Statistical image analysis of electron micrographs of ribosomal subunits. *Methods Enzymol.* **164**, 35–49.
20. Van Heel, M. & Frank, J. (1981) Use of multivariate statistics in analysing images of biological macromolecules. *Ultramicroscopy* **6**, 187–194.
21. Van Heel, M. (1989) Classification of very large electron microscopical image data sets. *Optik* **82**, 114–126.
22. Van Heel, M. (1987) Similarity between images. *Ultramicroscopy* **21**, 95–100.
23. Henderson, R.J., Baldwin, J.M., Downing, K.H., Lepault, J. & Zemlin, F. (1986) Structure of purple membrane from *Halobacterium halobium*: recording, measurement and evaluation of electron micrographs at 3.5 Å resolution. *Ultramicroscopy* **19**, 147–178.
24. Boekema, E.J., van Roon, H. & Dekker, J.P (1998) Specific association of photosystem II and light-harvesting complex II in partially solubilizedphotosystem II membranes. *FEBS Lett.* **424**, 95–99.
25. Boekema, E.J., van Breemen, J.F.L., van Roon, H. & Dekker, J.P. (2000) Conformational changes in photosystem II superomplexes upon removal of extrinsic subunits. *Biochemistry* **39**, 12907–12915.
26. Li, X.-P., Björkman, O., Shih, C., Grossman, A.R., Rosenquist, M., Jansson, S. & Niyogi, K. (2000) A pigment-binding protein essential for regulation of photosynthetic light harvesting. *Nature* **403**, 391–395.
27. The Arabidopsis Genome Initiative (2000) Sequence and analysis of the flowering plant *Arabidopsis thaliana*. *Nature* **408**, 796–815.
28. Boekema, E.J., Nield, J., Hankamer, B. & Barber, J. (1998) Localization of the 23 kDa subunit of the oxygen evolving complex of photosystem II by electron microscopy. *Eur. J. Biochem.* **252**, 268–276.
29. Nield, J., Funk, C. & Barber, J. (2000) Supermolecular structure of photosytem II and location of the PsbS protein. *Phil. Trans. R. Soc. London* **29**, 1337–1344.